© 2017. Published by The Company of Biologists Ltd | Development (2017) 144, 3253-3263 doi:10.1242/dev.153841

RESEARCH ARTICLE

Cytoskeletal variations in an asymmetric cell division support diversity in nematode sperm size and sex ratios

Ethan S. Winter[1,*], Anna Schwarz[2,*], Gunar Fabig[2,*], Jessica L. Feldman[3,*], André Pires-daSilva[4], Thomas Müller-Reichert[2], Penny L. Sadler[1,5] and Diane C. Shakes[1,‡]

ABSTRACT

Asymmetric partitioning is an essential component of many developmental processes. As spermatogenesis concludes, sperm are streamlined by discarding unnecessary cellular components into cellular wastebags called residual bodies (RBs). During nematode spermatogenesis, this asymmetric partitioning event occurs shortly after anaphase II, and both microtubules and actin partition into a central RB. Here, we use fluorescence and transmission electron microscopy to elucidate and compare the intermediate steps of RB formation in *Caenorhabditis elegans*, *Rhabditis* sp. SB347 (recently named *Auanema rhodensis*) and related nematodes. In all cases, intact microtubules reorganize and move from centrosomal to non-centrosomal sites at the RB-sperm boundary whereas actin reorganizes through cortical ring expansion and clearance from the poles. However, in species with tiny spermatocytes, these cytoskeletal changes are restricted to one pole. Consequently, partitioning yields one functional sperm with the X-bearing chromosome complement and an RB with the other chromosome set. Unipolar partitioning may not require an unpaired X, as it also occurs in XX spermatocytes. Instead, constraints related to spermatocyte downsizing may have contributed to the evolution of a sperm cell equivalent to female polar bodies.

KEY WORDS: Asymmetric partitioning, Spermatogenesis, X chromosome segregation, Cytoskeletal reorganization, Non-centrosomal microtubules, *Caenorhabditis elegans*, Spermiogenesis

INTRODUCTION

The asymmetric partitioning of cellular components along one or more axes is a crucial step in the differentiation of most cells (Nance and Zallen, 2011; Campanale et al., 2017). The resulting cell polarity is essential for proper cell function including motility in diverse cell types and the barrier function of epithelial cells; disruption of cell polarity is a hallmark of epithelial cancers (Halaoui and McCaffrey, 2015). Furthermore, cells can couple the establishment of cellular asymmetries with an oriented cell division to generate daughter cells with developmentally distinct cell fates.

[1]Department of Biology, College of William and Mary, Williamsburg, VA 23187, USA. [2]Experimental Center, Medical Faculty Carl Gustav Carus, Technische Universität Dresden, Dresden, 01307, Germany. [3]Department of Biology, Stanford University, Stanford, CA, 94305, USA. [4]School of Life Sciences, University of Warwick, Coventry, CV4 7AL, UK. [5]Department of Biology & Biochemistry, University of Houston, Houston, TX, 77204, USA.
*These authors contributed equally to this work

‡Author for correspondence (dcshak@wm.edu)

D.C.S., 0000-0002-9677-5577

Received 26 April 2017; Accepted 14 August 2017

During sperm development, asymmetric partitioning plays yet another role; it streamlines sperm for optimal motility. Mature sperm are small and motile, and thus one key step in their differentiation is the post-meiotic shedding of organelles and cytoplasmic components that are either unnecessary for or detrimental to subsequent sperm function (Fig. 1A). This shedding event involves two steps: (1) the differential partitioning of cellular components into a cellular wastebag known as a residual body (RB), and (2) the subsequent separation of this RB from the sperm (Steinhauer, 2015). In *Drosophila* and vertebrates, RB formation requires both actin and microtubules (Steinhauer, 2015; O'Donnell et al., 2001) and occurs as the final step of a post-meiotic cell differentiation process (spermiogenesis) that takes days to weeks and requires extensive cytoskeletal remodeling (Fabian and Brill, 2012; Clermont, 1972; Fig. 1A). In *C. elegans*, sperm production is accelerated by the production and pre-packaging of sperm components prior to the meiotic divisions; as a result, the highly reduced post-meiotic phase takes only minutes (Ward et al., 1981; Shakes et al., 2009; Chu and Shakes, 2013; Fig. 1B). Key to the brevity of this post-meiotic phase, RB formation occurs immediately after anaphase II and involves the replacement rather than the remodeling of cytoskeletal components (Fig. 1B; Shakes et al., 2009). Post-anaphase II, components required for sperm function, such as the fibrous body-membranous organelles (FB-MOs) partition to the haploid sperm whereas unneeded components are discarded into the RB that forms between the two sperm (Ward et al., 1981; Ward, 1986; Fig. 1D). Importantly, the discarded material includes the cell's entire store of actin and microtubules, as nematode sperm motility is driven not by a flagellum but by the assembly/disassembly dynamics of a nematode-specific cytoskeletal protein, the major sperm protein (MSP) (Smith, 2006; Yi et al., 2009).

It is unclear how the actin and microtubules in *C. elegans* spermatocytes shift from their anaphase II patterns to their final deposition within RBs or how various organelles differentially partition between the sperm and RB. In pharmacological studies, actin but not microtubule inhibitors block *C. elegans* sperm formation (Nelson et al., 1982). Genetic studies likewise implicate a key role for actin; mutants lacking the actin-binding protein SPE-26 fail to form RBs (Varkey et al., 1995), and loss of the unconventional myosin (myosin VI) specifically disrupts stable partitioning of actin, tubulin, mitochondria and FB-MOs (Kelleher et al., 2000). However, microtubules might also play a role as centrioles seem to specify the number and position of the sperm-RB boundaries (Peters et al., 2010). The associated transition from anaphase II to post-meiotic RB formation (Fig. 1B) is rapid and dramatic. Yet, little is known about the intermediate steps. Does nematode RB formation employ cellular mechanisms common to other asymmetric partitioning processes? Alternatively, given its unusually close juxtaposition to anaphase, has RB formation co-opted elements of the normal cytokinesis machinery?

Development (2017) 144, 3253-3263 doi:10.1242/dev.153841

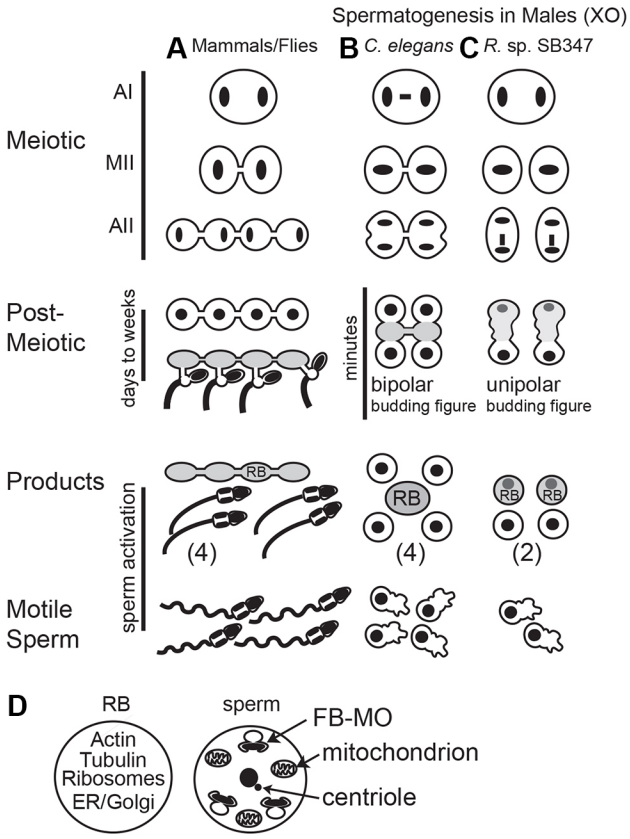

Fig. 1. Patterns of cell division and asymmetric partitioning during spermatogenesis. (A) In *Drosophila* and vertebrates, spermatocytes divide meiotically while connected by cytoplasmic bridges. After meiosis, the haploid sperm reassemble nuclear envelopes and differentiate into mature sperm. In a final step, unneeded cellular components partition into residual bodies (gray) as individual sperm separate from their cytoplasmic connections. Sperm acquire motility in a subsequent activation step. (B) In *C. elegans* males, the unpaired X chromosome (central bar) in anaphase I (AI) spermatocytes lags before segregating to one of the two secondary spermatocytes, which often remain connected by cytoplasmic bridges. Anaphase II (AII) is immediately followed by partitioning of unneeded components into a central (gray) residual body (RB) and then separation of the sperm from the RB. During this transition, the chromatin compacts and remodels but never reassembles a nuclear envelope (Ward et al., 1981; Shakes et al., 2009). Within the *C. elegans* literature, these newly separated, spherical sperm are typically called spermatids whereas the activated crawling sperm with their extended pseudopods are called spermatozoa. (C) In *R.* sp. SB347 males, spermatocytes undergo complete cytokinesis, generating unlinked secondary spermatocytes. Unpaired X chromosomes segregate as sister chromatids in anaphase I, while unpaired X chromatids (bar) lag during anaphase II (Shakes et al., 2011). Components required for sperm function then partition to the functional X-bearing sperm and unneeded components segregate to the RBs (gray), which includes the non-X chromosome set. (D) Schematic showing how cellular components are ultimately partitioned between the *C. elegans* RB and sperm.

The speed and relative simplicity of these post-meiotic events, combined with a striking degree of interspecies diversity in sperm size (Vielle et al., 2016), sperm morphology (Justine, 2002; Yushin and Malakhov, 2014) and patterns of sex chromosome segregation (Shakes et al., 2011), makes nematodes a valuable system for comparative studies. We recently described spermatogenesis in a nematode, provisionally named *Rhabditis* sp. SB347 and more recently designated *Auanema rhodensis* (Kanzaki et al., 2017), in which the unusually small spermatocytes of XO males do not form traditional RBs (Shakes et al., 2011; Fig. 1C). Instead, the asymmetric partitioning process yields functional, X-bearing sperm containing the essential sperm components and an RB containing the actin, tubulin and the non-X chromosome set. Crucial to this sex-biased gamete production, the unpaired X chromosome in the XO male spermatocytes of *R.* sp. SB347 does not lag during anaphase I as in *C. elegans* male spermatocytes (Albertson and Thomson, 1993; Fig. 1B). Instead, the X splits into sister chromatids during anaphase I, and the secondary spermatocytes always have a lagging X chromatid during anaphase II (Shakes et al., 2011; Fig. 1C).

In this study, we explore the cellular mechanisms of this asymmetric partitioning process through a comparative study of spermatogenesis in *C. elegans*, *R.* sp. SB347, and additional members of the *R.* sp. SB347 clade. Using a combination of fluorescence and transmission electron microscopy (TEM), we examine how sequential changes in microtubule and microfilament patterns correlate with the timing of anaphase chromosome segregation and the differential partitioning of specific organelles. We find that organelle partitioning occurs in two phases, with larger organelles partitioning early and endoplasmic reticulum (ER) partitioning only later during the final stages of sperm-RB separation. We identify the transition between anaphase II chromosome segregation and post-meiotic RB formation as the critical period when microtubules begin to reorganize and move from the centrosomes to the RB-sperm boundaries, and actin reorganizes to the RB through a combination of cortical ring expansion and clearance from the poles. In *R.* sp. SB347 and near relatives with similarly small spermatocytes, we find that the conversion of a typically bipolar partitioning process becomes unipolar, through the selective inactivation of one centrosome and differential clearing of actin from that same pole. Although we previously hypothesized that unipolar partitioning in *R.* sp. SB347 required an unpaired X during anaphase II (Shakes et al., 2011), we show here that both male (XO) and hermaphrodite (XX) spermatocytes divide in a unipolar fashion. The routine production during meiosis of functional and degenerate sperm during meiosis has been previously reported in rotifers (Whitney, 1918), aphids (Honda, 1921) and honeybees (Sharma et al., 1961). However, to our knowledge, this is the first example in nematodes of diminutive spermatocytes generating fewer than four functional gametes from meiosis and co-opting the process of RB formation to discard half of their genetic material into what appears to be the spermatogenesis equivalent of female polar bodies.

RESULTS

In *C. elegans* spermatocytes, intact microtubules reorganize and move from the centrosomes to the RB-sperm boundaries

During *C. elegans* spermatogenesis, the transition from anaphase II to post-meiotic RB formation and release includes a dramatic reorganization of the microtubule cytoskeleton from an anaphase spindle into non-spindle microtubules within the RB (Ward et al., 1981; Ward, 1986; Shakes et al., 2009). Yet the nature of this transition has been unclear. Are pre-existing microtubules reorganized or are they completely disassembled and newly reassembled within the RB? To understand the nature of this reorganization and whether it co-opts elements of the normal cytokinesis machinery, we imaged both live *C. elegans* spermatocytes using differential interference contrast (DIC) optics and fixed spermatocytes that had been co-labeled with DAPI and anti-α-tubulin antibodies (Fig. 2A). From anaphase I until early anaphase II, chromosomes segregated on typical microtubule spindles. Anaphase I spermatocytes were distinguished by the presence of a lagging X bivalent (blue arrow), which are known to

Development (2017) 144, 3253-3263 doi:10.1242/dev.153841

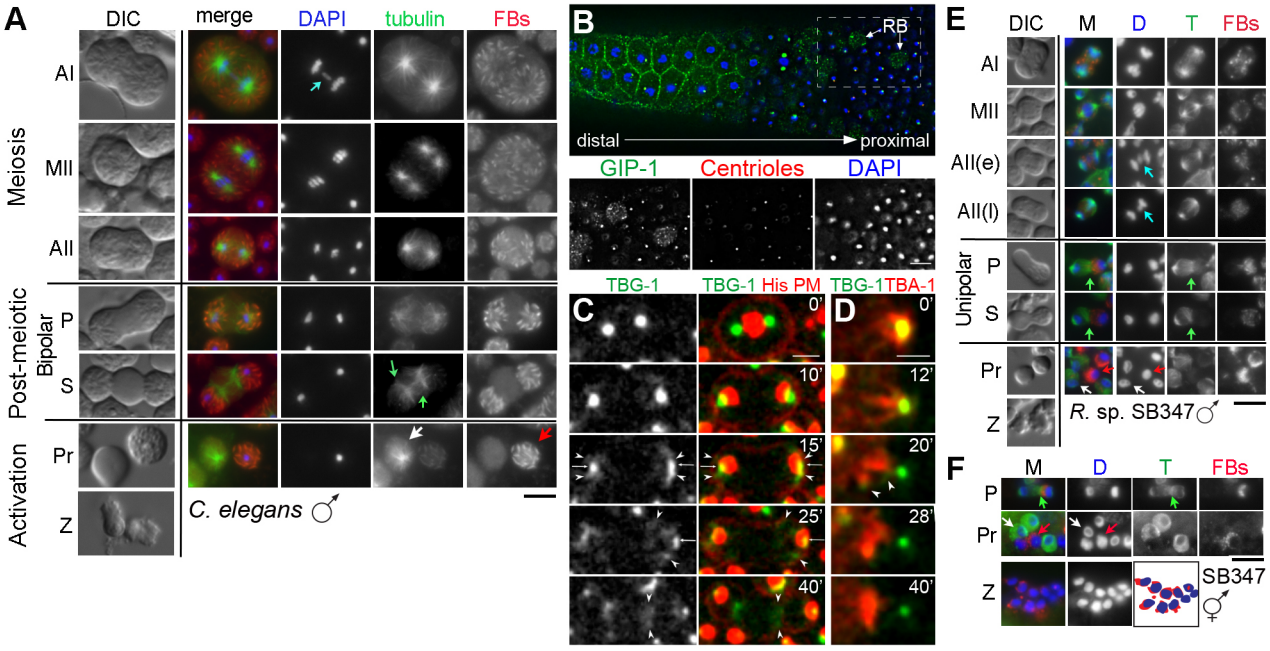

Fig. 2. Microtubule dynamics and organelle partitioning during spermatogenesis in *C. elegans* and *R.* sp. SB347. (A-F) Live and/or fixed cells from *C. elegans* males (A-D), *R.* sp. SB347 males (E) and *R.* sp. hermaphrodites (F). (A,E,F) Fixed cells in which the DNA is labeled with DAPI (blue), the microtubules with anti-α-tubulin antibodies (green), and the fibrous bodies (FBs) with anti-MSP antibodies (red). Light blue arrows in DAPI columns show an unpaired X chromosome lagging during anaphase I in *C. elegans* male spermatocytes (A) and an unpaired X chromatid lagging during anaphase II in *R.* sp. SB347 male spermatocytes (E). Green arrows show new secondary microtubule foci (green). Left column in A and E shows same stage live cells imaged under DIC optics. (B) Fixed male gonad from *C. elegans.* DNA is labeled with DAPI (blue), endogenous GIP-1 with anti-GIP-1 antibodies (green), and centrioles with anti-IFA antibodies (red). Top image shows a developmental progression of spermatocytes in meiotic prophase on the left (distal) side and intermixed RBs (arrows) and sperm on the proximal side. Single-channel images of the boxed region are shown below. (C) Images of a live metaphase II spermatocyte transitioning to the separation phase showing the dynamics of γ-tubulin (GFP:TBG-1, green), chromosomes (histone:mCherry, red) and the cell membrane [mCherry:PH(PLC1δ1), red]. Small arrows indicate residual centrosomes. Arrowheads show non-centrosomal γ-tubulin. (D) Anaphase II to separation in a live spermatocyte expressing GFP:γ-tubulin (TBG-1, green) and mCherry:α-tubulin (TBA-1, red; time in minutes). Anaphase I (AI), metaphase II (MII), anaphase II (AII) post-meiotic partitioning (P) and separation (S) phases, the products (Pr) that include functional sperm (red arrows) and residual bodies (white arrows), and crawling spermatozoa (Z) are indicated. Scale bars: 5 µm.

ultimately segregate to one of the two secondary spermatocytes (Albertson and Thomson, 1993). However, as the haploid chromosome sets moved further apart and the spermatocytes elongated (partitioning phase, P), microtubules were no longer anchored at the centrosomes, and the DIC images revealed a central region lacking refractive FB-MOs. Once constrictions had formed between each sperm and the central RB (separation phase, S), microtubules had completely reorganized into two broad bands, one at each RB-sperm boundary. As the RB fully separated from the adjacent sperm products (Pr), the cortical ends of the microtubules gathered into discrete foci. Newly formed RBs had two or four discrete foci, depending on whether the secondary spermatocytes had fully separated after the first meiotic division.

As microtubules reorganize and move to the RBs, their centrioles remain with the sperm (Ward et al., 1981; Peters et al., 2010; Shakes et al., 2009). To understand how centrosomal microtubules reorganize into non-centrosomal microtubules, we examined microtubule localization and polarity in fixed and living cells. Microtubule minus ends were visualized by the localization and movement of TBG-1/γ-tubulin and GIP-1/GCP3, both components of the γ-tubulin ring complex (γ-TuRC) (Fig. 2B-D). In fixed preparations, γ-TuRC proteins localized to the cell cortex of developing spermatocytes before relocalizing to the centrosomes of spermatocytes that were initiating their meiotic divisions (Fig. 2B). Following the meiotic divisions, most of the γ-TuRC proteins relocalized to punctate structures in the RBs, although a subpopulation remained behind with the inactive centrosomes, as has been observed in other differentiated cell types (Feldman and Priess, 2012; Zhou et al., 2009; J.L.F., unpublished data).

In live metaphase II spermatocytes, GFP:TBG-1 localized exclusively to the centrosome (Fig. 2C, 0 min; Movie 1). However, as cells progressed beyond anaphase II, the centrosomes flattened and GFP:TBG-1 spread along the cortex (Fig. 2C, arrowheads). As spermatocytes elongated, some GFP:TBG-1 remained with the inactivated centrosome, whereas the non-centrosomal fraction of GFP:TBG-1 moved towards the RB, eventually concentrating at the RB-sperm boundary during the separation phase (40′). To assess microtubule reorganization directly, we also observed live spermatocytes co-expressing GFP:TBG-1 and mCherry:TBA-1 (α-tubulin, a core subunit of microtubules) (Fig. 2D, Movie 2). Localization of GFP:TBG-1 to the cortical tips of microtubules (arrowheads, 20′) suggests that microtubules remain intact and associated with their γ-TuRCs as they move to the RBs, and orient with their minus ends specifically abutting the RB-sperm boundaries.

In *R.* sp. SB347 male spermatocytes, major shifts in microtubule patterns are confined to the single, X-bearing pole

In *R.* sp. SB347 spermatocytes, microtubule organization was initially similar to that in *C. elegans* (Fig. 2E). However, by early anaphase II [AII(e)] when microtubule asters were already at the two poles, the spermatocytes were only slightly elongated, and the X

Development (2017) 144, 3253-3263 doi:10.1242/dev.153841

chromatid was centrally positioned. As long as the X remained centrally positioned, the microtubule spindles were symmetric (35/35). However by late anaphase II [AII(l)], when the X had physically contacted but not yet fully incorporated into one anaphase plate, the spindles were asymmetric (62/68) with long microtubules emanating from the X-bearing pole. Although late anaphase II spermatocytes with symmetric spindles were observed, they were not only rare but were associated with individual males who had multiple such spermatocytes, suggesting that they represented worm-to-worm variation rather than standard intermediates. All other late anaphase II spermatocytes exhibited dramatic intra-spindle size asymmetry. This type of spindle asymmetry, in which the two half-spindles vary dramatically in length, has been shown to mechanistically support asymmetric, mitotic cell divisions in many other organisms and contexts (Knoblich, 2010; Delaunay et al., 2014).

After the X chromatid had fully incorporated into one haploid chromosome set (Fig. 2E) and the cells entered the post-meiotic partitioning (P) and separation (S) phases, microtubule reorganization occurred specifically at the X-bearing pole. At this point, the chromosomes were farther apart, the cells had elongated, and same-stage DIC images showed a clearing of refractive bodies from one pole, which other studies have determined to be the non-X pole (Shakes et al., 2011). Remarkably, as microtubules from the X-bearing pole reorganized and moved to the single RB-sperm boundary (Fig. 2E, green arrows, unipolar), microtubule asters at the non-X pole remained relatively unchanged. In summary, a process of microtubule reorganization and centrosome inactivation that is bipolar in *C. elegans* (Fig. 2A) is unipolar in *R.* sp. SB347 (Fig. 2E).

In both *C. elegans* and *R.* sp. SB347, asymmetric FB-MO partitioning coincides with post-meiotic events

The major sperm protein (MSP) is a cytoskeletal protein that ultimately drives nematode sperm motility; however, when MSP is first synthesized, it is packaged in the form of paracrystals within discrete fibrous bodies (FBs) (Smith, 2006). To determine whether asymmetric FB partitioning coincides with either chromosome segregation or microtubule reorganizaton, FB patterns were examined in co-labeled spermatocytes. In fixed *C. elegans* spermatocytes, FBs were uniformly distributed until the completion of anaphase II, at which point the FBs began clearing from the cell center (Fig. 2A). In spermatocytes in which microtubules were actively reorganizing and moving centrally to the RB-sperm boundaries, FBs were already in place within the sperm and no longer in the expanding RB.

In meiotically dividing *R.* sp. SB347 spermatocytes, FBs were symmetrically distributed, while being specifically excluded from both the metaphase plate and the anaphase poles (Fig. 2E). Contrary to our earlier predictions (Shakes et al., 2011), FB partitioning did not coincide with either X chromatid segregation or establishment of the asymmetric spindle; FBs remained centrally located, regardless of whether the lagging X was positioned centrally (11/11) [Fig. 2E, AII(e)] or loosely associated with one pole (32/32) [Fig. 2E, AII(l)]. Instead, FB partitioning coincided with the X fully incorporating into an anaphase plate. In 33/37 spermatocytes in which a distinct X was no longer detectable, the FBs had asymmetrically partitioned to the pole with the larger, X-bearing chromatin mass (Fig. 2E, P). The process of FB partitioning is presumably rapid as we failed to identify partitioning intermediates. In contrast, microtubules reorganized throughout the partitioning phase. The unpaired X in *R.* sp. SB347 effectively prolongs anaphase II, strongly suggesting that FB partitioning in *R.* sp. SB347, and presumably in *C. elegans*, coincides not with anaphase chromosome segregation but with anaphase completion and the movement of microtubules away from the X-bearing pole. This model is consistent with earlier proposals that RB formation in nematodes should be considered part of post-meiotic sperm differentiation (spermiogenesis) rather than part of the meiotic divisions (Shakes et al., 2009; Chu and Shakes, 2013).

Unipolar partitioning also occurs during spermatogenesis in XX *R.* sp. SB347 hermaphrodites

In *R.* sp. SB347 males, the partitioning of sperm essential components specifically to the X-bearing sperm suggested that the unpaired X chromatid might physically cue the asymmetry (Shakes et al., 2011). If so, the production of functional and non-functional sperm should be an exclusive property of XO males, because only XO secondary spermatocytes are predicted to have an unpaired X. We hypothesized that, in the absence of an unpaired X, spermatocytes from XX hermaphrodites would undergo bipolar partitioning to produce four functional sperm and an RB without DNA. Contrary to our expectations, hermaphrodite spermatogenesis yielded a mixture of DNA-containing (MSP negative, tubulin positive, white arrow) RBs and functional (MSP positive, tubulin negative, red arrow) sperm (Fig. 2F, Pr; 100% of >30 hermaphrodites scored at this stage). Furthermore, although they were difficult to capture, all observed post-meiotic intermediates (8/8 cells) exhibited unipolar partitioning (Fig. 2F, P). Thus, the unipolar division that generates one functional sperm and one DNA-containing RB during *R.* sp. SB347 spermatogenesis occurs in both XX and XO germlines.

Post-meiotic, asymmetric partitioning occurs in two discrete phases

Whereas FB-MOs and mitochondria partition to the sperm, other organelles such as the ER partition to the RB (Ward et al., 1981; Fig. 1D). To assess the relative timing of ER partitioning, we examined ER in fixed spermatocytes using an antibody against the ER-specific cytochrome P450 marker, CYP-33E1 (Hadwiger et al., 2010). In *C. elegans* meiotic spermatocytes, CYP33-E1 labeled both a diffuse cytoplasmic component and discrete, elongated tube-like structures that were distributed throughout the cell (Fig. 3A). During the post-meiotic stages (P, S), the diffuse cytoplasmic component localized to the expanding RB, whereas the tubular structures remained uniformly distributed throughout most of the separation phase before ultimately partitioning to the RBs (white arrow). During *R.* sp. SB347 spermatogenesis, CYP33-E1 exhibited an analogous pattern (Fig. 3B). The diffuse component partitioned away from the X-bearing sperm at the beginning of the post-meiotic stage, whereas the faintly labeled tubular structures partitioned to the RB (white arrow) only later. The molecular forces involved in partitioning these late-segregating components remains unclear.

Transmission electron micrographs of *R.* sp. SB347 spermatocytes

Because the small size of the *R.* sp. SB347 spermatocytes made it challenging to visualize details of the partitioning process, we further investigated the relative timing of these events using thin section electron microscopy. In cells in which the X chromatid (marked in orange) was positioned in between the autosomes (marked in blue), the mitochondria and FB-MO complexes seemed to be equally distributed (Fig. 3C). In cells in which the X chromatid had fully incorporated into an anaphase plate, FB-MOs and mitochondria were differentially partitioned to the X-bearing pole (Fig. 3D). During these early stages, tubular and membranous structures as well as ribosomes remained evenly distributed

Development (2017) 144, 3253-3263 doi:10.1242/dev.153841

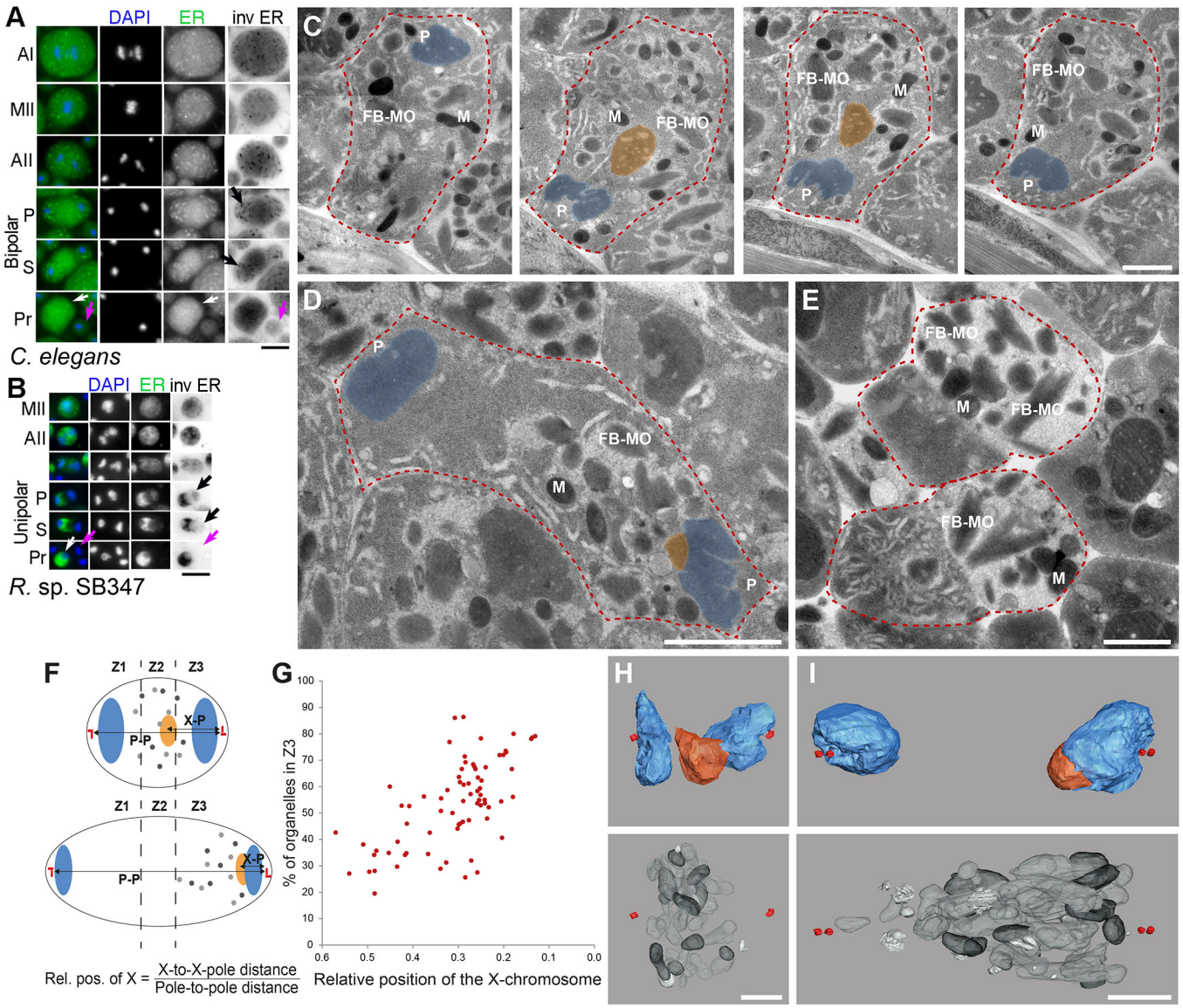

Fig. 3. Differential organelle partitioning in *R.* sp. SB347 spermatocytes. (A,B) Fixed and staged male spermatocytes labeled with DAPI (blue) and the anti-ER antibody CYP-33E1 (green) from *C. elegans* (A) and *R.* sp. SB347 (B). Cell stage labels as in Fig. 2. White arrows indicate RB product and purple arrows functional sperm after separation. In the inverted (inv) image, the bright CYP-33E1-labeled tubules are now black on a white background. Black arrows show late-clearing, CYP-33E1-labeled tubules. (C-E) Thin section EM images of four sections through the same cell in early anaphase II (C), a cell in post-meiotic partitioning phase (D) and two cells in the separation phase (E). Cell outlines are shown as red dashed line, autosomes in light blue, lagging X chromosome in red. Spindle pole (P), mitochondrion (M), fibrous body-membranous organelle (FB-MO) are indicated. The granular structure is due to the ribosomes. (F) Schematic of the analysis procedure carried out for 76 cells in meiosis II. Organelles are represented by different colored dots: FB-MOs (light gray) and mitochondria (dark gray). Red bars represent the centrioles of each centrosome. P, pole. (G) Quantitative analysis of FB-MO and mitochondria partitioning in male spermatocytes relative to the position of the X chromatid. (H,I) 3D models from serial electron tomographic reconstructions of a cell in early anaphase II (H) and one in early partitioning (I). Images show centrioles (red dots), autosomes (blue), the X chromatid (orange), FB-MOs (light gray), mitochondria (dark gray) and Golgi (white). Scale bars: 5 µm (A,B); 1 µm (C-E,H,I).

(Fig. 3C,D), and they only differentially partitioned to the RB near the end of the separation stage (Fig. 3E).

In parallel studies, we analyzed serial ‘semi-thick’ (300 nm) sections, which enabled us to capture the entire volume of dividing spermatocytes. Analysis of 76 anaphase II and partitioning phase cells within six different individuals enabled us to quantify the asymmetric partitioning of the mitochondria and FB-MOs relative to the cells’ progression through anaphase II (Fig. 3F,G). Within individual secondary spermatocytes, the number of organelles per cell was counted and assigned to one of three defined zones: closer to the centrosome without the X chromosome (Z_1), closer to the centrosome associated with the X chromosome (Z_3), or in a zone in between (Z_2) (Fig. 3F). Because individual cells differed in size and shape, we normalized the X chromosome to X-bearing centrosome distance (X-to-X-pole distance) to the centrosome-to-centrosome distance (pole-to-pole distance). Plotting X chromatid position against the fraction of organelles in Z_3 revealed that most FB-MOs and mitochondria partitioned only once the X approached the relative position of 0.2 and thus was mostly or fully incorporated into one of the anaphase plates (Fig. 3G).

Using electron tomography, we also fully reconstructed two cells, one in early anaphase II and one in early partitioning (Fig. 3H,I).

Development (2017) 144, 3253-3263 doi:10.1242/dev.153841

When the X chromatid was positioned centrally (Fig. 3H), so were the FB-MOs (light gray), mitochondria (dark gray) and, when scorable, Golgi complexes (white). When the X segregated to one pole and was nearly or fully incorporated into the chromosome cluster (and would have been scored as fully incorporated by DAPI staining), the FB-MOs and mitochondria were restricted to the X-bearing side (Fig. 3I). In contrast, Golgi complexes (white) within this same cell remained symmetrically distributed. These same three-dimensional reconstructions enabled us to obtain precise counts of organelle numbers; we counted 27 FB-MOs and 11 mitochondria within the anaphase II spermatocyte, and 34 FB-MOs and 14 mitochondria within the partitioning-stage spermatocyte.

Unipolar partitioning occurs in other trioecious species of the *R.* sp. SB347 clade but not in the male/female species *Rhabditella axei*

To determine whether the unipolar partitioning process that yields one functional sperm and one DNA-containing RB from each *R.* sp. SB347 secondary spermatocyte represents an evolutionary oddity or a characteristic feature of this clade (Fig. 4A), we investigated male spermatogenesis in closely related species that, like *R.* sp. SB347, are both trioecious (males/females/hermaphrodites) and have small sperm. *Rhabditis* sp. SB372 males have sperm (4.6±0.9 μm^2 cross-sectional area) that are slightly smaller than those of *R.* sp. SB347 males (6.7±1.6 μm^2) and much smaller than those of *C. elegans* (15.2±2.5 μm^2). *R.* sp. SB372 spermatocytes (Fig. 4B,C) shared many similarities with those of *R.* sp. SB347. Primary spermatocytes divided symmetrically, and we found no evidence of lagging X chromosomes during anaphase I. Although difficult to see in these smaller spermatocytes, we routinely observed a central, lagging X chromatid during meiosis II (Fig. 4B, yellow arrow) and were able to distinguish the X-bearing pole at later stages by its larger chromatin mass. The meiotic spindle became asymmetric as the X chromatid moved to one pole (Fig. 4B, AII,P). Microtubules from the X-bearing pole subsequently shifted to the RB-sperm boundary during separation (Fig. 4B, S). FB partitioning began in late anaphase II and continued through partitioning (Fig. 4C, P). Ultimately, the microtubules partitioned to the RBs (green arrow) whereas the FBs partitioned to the X-bearing sperm (Fig. 4C, white arrow). We observed similar patterns in the even smaller sperm (4.3±0.6 μm^2) of *R.* sp. JU1783 males (Fig. 4D,E). However, the functional sperm of *R.* sp. JU1783 males often retained small amounts of α-tubulin, presumably associated with the centrosome (Fig. 4D, Pr), and some males produced a mix of tubulin-enriched cytoplasts both with and without chromatin (green arrows), suggesting the production of some 'traditional' RBs without chromatin.

To determine whether unipolar partitioning was characteristic of this entire clade or restricted to trioecious relatives, we also examined spermatocyte partitioning in *Rhabditella axei*, the closest known male/female relative of *R.* sp. SB347 (Kiontke and Fitch, 2005). As in other male/female nematodes, *R. axei* males have much larger sperm (60.1±7.3 μm^2). Furthermore, their spermatocyte divisions yield four functional sperm (Shakes et al., 2011). Immunostained preparations of *R. axei* spermatocytes revealed patterns both similar to and distinct from those in either *C. elegans* or *R.* sp. SB347 (Fig. 4F). As previously reported (Shakes et al., 2011), the male spermatocytes in *R. axei* exhibit the same X chromosome segregation patterns as in *R.* sp. SB347 and thus have lagging X chromatids during anaphase II (Fig. 4F, yellow arrow and full-sized DAPI images on right). Yet unlike those in *R* sp. SB347, *R. axei* meiotic spindles remained symmetric throughout anaphase II. During the meiotic divisions, FBs distributed uniformly throughout the spermatocytes. FBs began clearing (purple arrow) from the central region, after the completion of anaphase II (P). By the time the chromosome sets had compacted into tight single masses (orange arrow), microtubules had fully reorganized and moved to the RB-sperm boundaries. A unique feature of *R. axei* spermatogenesis is that, although we observed pairs of sperm separating from a central RB (S**, offset DIC image at the bottom of Fig. 4F), the meiosis II cleavage furrow often proceeded to completion, generating two large, polarized sperm that each subsequently generated their own RB (Fig. 4F, S*,Pr). Despite this altered cleavage pattern, the relative timing of polarization events in *R. axei* spermatocytes is the same as in *C. elegans* and *R.* sp. SB347. Furthermore, these studies confirm that, despite having

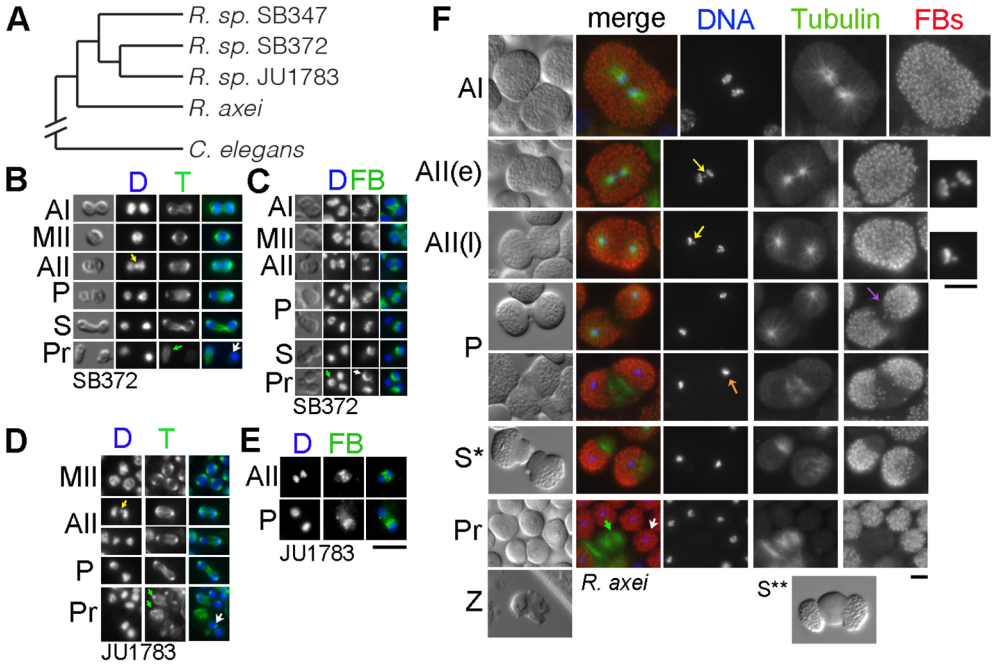

Fig. 4. Microtubule patterns and FB partitioning in *R.* sp. SB347 near relatives. (A) Molecular phylogeny of near relatives (Kanzaki et al., 2017). (B-F) Fixed spermatocytes and sperm from *R.* sp. SB372 (B,C), *R.* sp. JU1783 (D,E), and *R. axei* (F) labeled with DAPI (blue) and antibodies against either α-tubulin (T) or MSP (FBs) in same cell (B,C) or same-stage (F) DIC images in the left column. Cell stages as in Fig. 2. *R. axei* sperm that have (S*) or have not (S**) separated from each other before secondarily separating from residual body components are also shown. Arrows label lagging X chromatid (yellow), X-bearing sperm (white), RBs with or without a chromatin mass (green), FB clearing (purple), and chromosomes compacting into a single mass (orange). Scale bars: 5 μm. Sperm size measurements calculated from >5 gonads, 20-30 sperm/gonad.

Development (2017) 144, 3253-3263 doi:10.1242/dev.153841

an X chromosome segregation pattern like *R.* sp. SB347, microtubule reorganization and FB partitioning in these much larger *R. axei* spermatocytes is bipolar as in *C. elegans*.

Actin microfilaments reorganize through a combination of cortical ring broadening and clearing from one or both poles

In all of these species, FB-MOs asymmetrically partition post-meiotically as the cells elongate and the microtubules reorganize and move to the RB-sperm boundary. But what forces establish this polarity and direct the movement of these organelles? In *R.* sp. SB347 male spermatocytes, the late anaphase II spindle asymmetry may help establish the initial polarity, but FB-MO partitioning occurs only later as the microtubules are reorganizing at the X-pole. Furthermore, when we assessed the proximity of mitochondria and FB-MOs to adjacent microtubules in our TEM studies, the distances were too great to be bridged by microtubule motors (data not shown). Alternatively, a key role for actin would be consistent with earlier pharmacological and genetic studies in *C. elegans* (Nelson et al., 1982; Kelleher et al., 2000). However, few details were known about the step-wise changes in the actin cytoskeleton as nematode spermatocytes progress from anaphase II and through the early post-meiotic partitioning events.

In fixed *C. elegans* spermatocytes, microfilaments were present around the entire cortex during the meiotic divisions, but an enhanced cortical ring developed during anaphase I and II (Fig. 5A, white arrows). During anaphase II, a defined ring could only be observed when the chromosomes were still fairly close together. As the spermatocytes elongated and transitioned to the post-meiotic partitioning phase (P), the central ring widened into a band (white asterisk). At the same time or shortly thereafter, microfilaments progressively cleared from the poles (orange arrows). By the separation phase, microfilaments were completely restricted to the RB, both at the cortex and within the RB cytoplasm. Separated RBs exhibited actin patches at what we assume are the former sperm attachment sites (green arrows) suggesting a potential role for actin in RB-sperm abscission.

In the larger *R. axei* spermatocytes, actin patterns were similar but more exaggerated (Fig. 5B). During anaphase II, microfilaments were initially present both at the cortex and in a central cortical ring (white arrows). As the spermatocyte elongated, the central actin ring expanded in the form of a gradient (P), and microfilaments progressively cleared from the poles (orange arrows). As the microfilaments continued to clear from the poles, those within the RB were no longer confined to the cortex but broadly distributed throughout.

R. sp. SB347 spermatocytes exhibited a unipolar version of these same events (Fig. 5C). In metaphase spermatocytes, microfilaments distributed uniformly around the cortex (data not shown), but during anaphase II, they differentially accumulated in a central cortical ring (white arrow). Once the lagging X chromatid fully incorporated into an anaphase plate, microfilaments specifically cleared from the cortex of the X-bearing pole (orange arrows). Throughout the partitioning phase, microfilaments remained at the RB cortex and established a concentrated central band (purple arrows) adjacent to the RB-sperm boundary. In detached RBs, microfilaments distributed throughout the cytoplasm. Although these observations do not directly test whether actin functions in FB partitioning, they are consistent with either actin or actomyosin forces functioning to physically exclude larger organelles from the RB.

DISCUSSION

How nematode spermatocytes generate haploid sperm lacking both actin and tubulin has always been an intriguing cellular phenomenon,

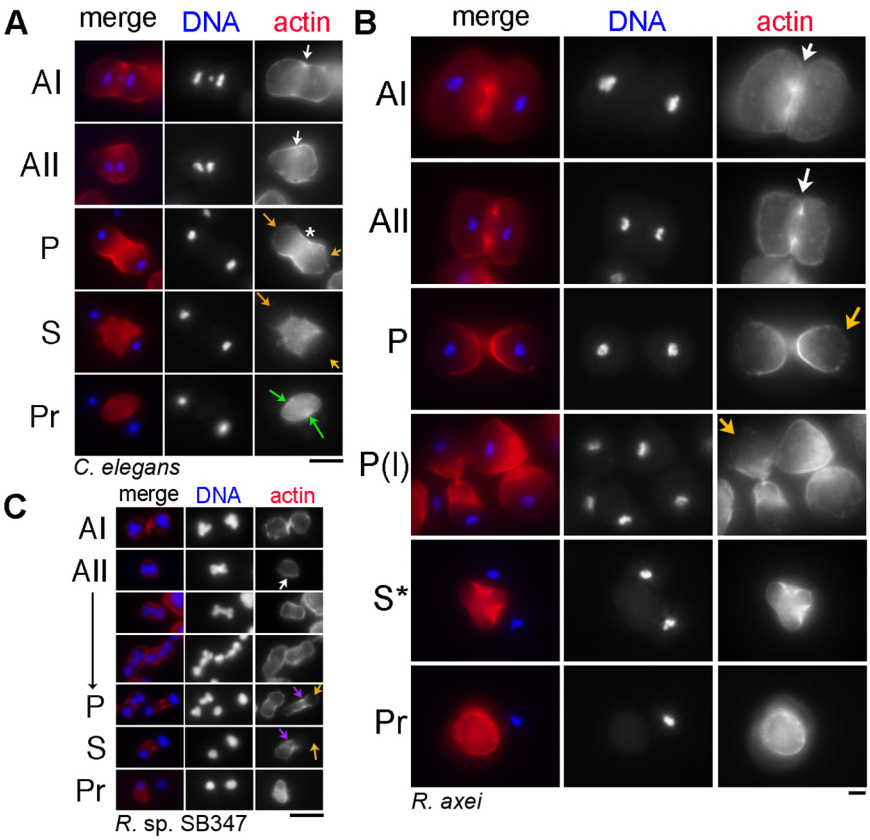

Fig. 5. Actin patterns during *C. elegans*, *R. axei* and *R.* sp. SB347 spermatogenesis. Fixed spermatocytes and sperm labeled with DAPI (blue) and rhodamine-phalloidin (red) from *C. elegans* (A), *R. axei* (B) and *R.* sp. SB347 males (C). (C) A physical chromatin connection between X chromatid and the autosomes was apparent throughout anaphase II in the aldehyde-fixed specimens in both these and the TEM studies. Arrows indicate cortical actin ring (white), clearing of actin from one or both poles (orange), persistent cortical ring at the base of the X-bearing sperm (purple), and actin patches of residual body at former bud sites (green). Scale bars: 5 µm.

Development (2017) 144, 3253-3263 doi:10.1242/dev.153841

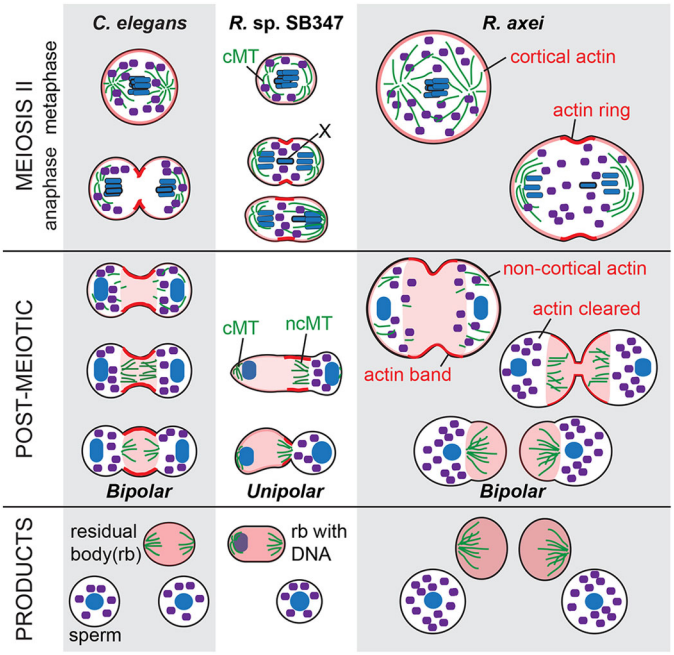

Fig. 6. Conserved and divergent aspects of cytoskeletal reorganization in diverse nematode spermatocytes. Comparative schematic of the differential partitioning events during residual body formation in *C. elegans*, *R.* sp. SB347 and *R. axei* spermatocytes. Actin microfilaments (red); centrosomal (c) or non-centrosomal (nc) microtubules (MT) (green); chromatin (blue); and large organelles (purple). X chromatids have heavy black outline.

yet little was known about how this cellular transformation was actually accomplished. Now, by comparing the sequence of cytoskeletal changes that accompany this transformation in diverse nematode spermatocytes, we have identified both conserved and divergent aspects of the process (Fig. 6).

One might assume that the cellular processes that enable a spermatocyte to discard its microtubule cytoskeleton would be unique to nematode spermatogenesis. However, our key finding that microtubules reorganize as they move from the centrosome to the RB-sperm boundary suggests a clear and informative parallel to similar centrosomal to non-centrosomal conversions in a wide range of differentiating cells including epithelial cells, neurons and oocytes (reviewed by Bartolini and Gundersen, 2006; Sanchez and Feldman, 2017). In these cases, the reassignment of microtubule organizing center (MTOC) function is postulated to involve the movement of microtubules directly from the centrosome to non-centrosomal sites, but direct evidence has been lacking. Our live-imaging studies suggest that intact microtubules move together with γ-TuRCs. This association would both stabilize the pre-existing microtubules and could enable nucleation of new microtubules from a repositioned MTOC. In the context of nematode spermatogenesis, this strategy could provide an efficient way of clearing tubulin from the sperm.

With some exceptions, such as in plant cells and meiotically dividing oocytes, non-centrosomal microtubules are typically restricted to differentiated, non-dividing cells as they appear to be inhibited by mitotic (and meiotic) kinases (Sallee and Feldman, 2015). Our studies reveal that *C. elegans* spermatocytes undergo two sequential transitions. During meiotic prophase, the microtubules are organized by cortically localized, non-centrosomal MTOCs. As spermatocytes initiate the meiotic divisions, MTOC function switches to the centrosomes before switching back to a non-centrosomal state at the end of anaphase II. In *R.* sp. SB347, this second switch is restricted to one pole. In male spermatocytes, the loss of centrosomal MTOC function occurs specifically at the X-pole as the lagging X incorporates into the anaphase plate; yet the same unipolar switch occurs in hermaphrodite spermatocytes which presumably lack a lagging X. In both *C. elegans* and *R.* sp. SB347, the centrosomal to non-centrosomal switch correlates with anaphase completion and a key step in sperm differentiation, the remodeling of chromosomes into a single tight chromatin mass. In *R. axei*, where these events occur sequentially, MTOC reassignment correlates with the later event of chromatin remodeling. In other developmental contexts, asymmetry in centrosome behavior is linked to cell fate. For example, asymmetric MTOC function at the centrosome allows for the selective retention of the daughter centrosome in *Drosophila* neuroblasts and of the mother centrosome (or spindle pole body) in *Drosophila* male germline stem cells, mouse radial glial cells and *Saccharomyces cerevisiae* bud cells (Yamashita et al., 2007; Wang et al., 2009; Conduit et al., 2010; Januschke et al., 2011; Pereira and Schiebel, 2001). We have yet to determine whether the non-X pole in *R.* sp. SB347 spermatocytes stereotypically associates with the mother or daughter centrosome, but the maintenance of an active centrosome MTOC within the developing RB suggests a similar link between centrosome asymmetry and cell fate.

Our actin results, showing (1) cortical ring broadening throughout anaphase and (2) actin clearing from the poles as spermatocytes elongate, also have parallels in other cell types. Efficient metaphase spindle assembly requires uniform cortical rigidity (Matthews et al., 2012) whereas mid-anaphase cell elongation requires relaxation at the poles through the localized loss or remodeling of actin microfilaments (Roubinet et al., 2011; Kunda et al., 2012; Rodrigues et al., 2015). Typically, this remodeling includes a minor reduction in actin microfilaments at the poles and localized deactivation of the actin-plasma membrane linker moesin. In nematode spermatocytes, the clearing of actin from one or both poles coincides with spermatocyte elongation and post-anaphase partitioning, but in its exaggerated form, it also provides a mechanism for clearing actin from the sperm.

In other systems, differential clearing of myosin from one pole creates an asymmetry in actin forces that shifts the cleavage furrow and generates an asymmetric cell division (Ou et al., 2010; Connell et al., 2011). In *C. elegans* spermatocytes, the combination of clearing of actin from both poles and accumulating actin centrally might create asymmetric actin forces that bi-directionally shift cleavage furrow activity away from the center and towards the two RB-sperm boundaries. Conversely, unipolar clearing in *R.* sp. SB347 may account for the single, displaced cleavage furrow. At the other extreme, stability rather than regression of the central cleavage furrow may be favored in the larger *R. axei* spermatocytes, such that they first cleave in two before the individual sperm secondarily separate from their RB. Future studies might show that a two-step process is typical for larger spermatocytes. Notably, our results indicate that *R. axei* spermatocytes still initiate partitioning immediately after completing anaphase II; only RB-sperm abscission is delayed.

Broadening of the actin cortical ring coupled with localized accumulation of non-cortical microfilaments may also facilitate both RB formation and separation. An expanding band of cortical actin could provide counterbalancing rigidity for spermatocyte elongation at the softened poles and support rounding up of the RB into a sphere, the shape of which is largely independent of the cytoplasmically linked sperm. Furthermore, because larger organelles (e.g. FB-MOs and mitochondria) in *R.* sp. SB347 and *R. axei* do not partition in association with microtubules, perhaps non-cortical microfilaments within the expanding RBs partition them through exclusion. During *Drosophila* spermatogenesis, an

Development (2017) 144, 3253-3263 doi:10.1242/dev.153841

actin meshwork functions in this manner. During RB formation and separation, often referred to as individualization, an actin cone moves down the length of the axoneme and an actin meshwork within excludes cytoplasm and organelles from the rest of the sperm (Fabrizio et al., 1998; Noguchi et al., 2006). Our finding that nematode RB formation is associated with post-anaphase II actin remodeling confirms its value as an informative parallel to RB formation in non-nematodes.

In *R.* sp. SB347 males, the production of two rather than four functional products from spermatocyte meiosis combined with the invariable segregation of the X to the functional sperm provides a convenient and evolutionarily useful mechanism for generating a feminine-biased sex ratio. Yet this study suggests that an unpaired X during anaphase II is neither sufficient nor necessary for this pattern of division. Despite having an unpaired X chromatid during anaphase II, the large spermatocytes of *R. axei* males yield four functional sperm with Mendelian 50:50 sex ratios. Conversely, the tiny spermatocytes in *R.* sp. SB347 XX hermaphrodites only yield two functional sperm, despite presumably having paired X chromosomes in both meiotic divisions. Tiny male spermatocytes in *R.* sp. SB347 near relatives typically yield two functional sperm and two DNA-containing RBs. In *R.* sp. SB372 males, these unipolar divisions also correlate with skewed sex, feminine-biased sex ratios (Kanzaki et al., 2017), but further studies of the other near relatives are needed to assess both their sex ratios and how often their RBs lack DNA. Collectively, our current data is consistent with the unpaired X in *R.* sp. SB347 male spermatocytes merely following the RB-sperm asymmetry, and that the crucial, shared feature of these modified unipolar divisions is not an unpaired X during anaphase II but the diminutive size of the spermatocytes.

What possible evolutionary advantage could be gained by throwing away half of one's potential sperm? Studies of nematode sperm size in both the genus *Caenorhabditis* and the family Rhabditidae suggest that sperm size is driven by two opposing factors. Larger sperm are more competitive (LaMunyon and Ward, 1999), and thus they are favored when sperm competition between genetically dissimilar males is high, as typically occurs in male/female species. However, the costs of producing larger sperm are that sperm production is slower and fewer sperm can be stored within the spermatheca for subsequent fertilization events (LaMunyon and Ward, 1999; Murray et al., 2011; Vielle et al., 2016). Therefore, small sperm are favored in hermaphroditic species where sperm competition is low and smaller sperm can be produced more quickly and stored in higher numbers (LaMunyon and Ward, 1999; Baldi et al., 2011). Within the family Rhabditidae, the sperm of *R.* sp. SB347 and its trioecious near relatives (this study) are the smallest reported to date (LaMunyon and Ward, 1999; Vielle et al., 2016; this study). We hypothesize that evolutionary pressures to reduce sperm size in *R.* sp. SB347 may have reached a cellular and developmental threshold. To function, the motile spermatozoa require a minimal stock of mitochondria and cytoplasmic components. Already, the thin shell of cytoplasm surrounding the DNA of *R.* sp. SB347 spermatozoa seems barely enough to support motility. Furthermore, the developmental program of spermatogenesis requires throwing away materials that could be detrimental for subsequent sperm function. Perhaps in *R.* sp. SB347 and its trioecious near relatives, the advantage of rapid sperm production outweighs the cost of throwing away haploid complements of genetic material. If so, these spermatocytes have effectively adopted a standard strategy of oocytes; producing functional sperm of the necessary size at the cost of discarding meiotic products within RBs, the spermatogenesis equivalent of oocyte polar bodies.

MATERIALS AND METHODS

Maintenance and origin of strains

All nematode strains were maintained on plates of MYOB agar (Church et al., 1995) or NGM agar (Brenner, 1974) seeded with the *Escherichia coli* uracil auxotroph mutant strain OP50. Strains were maintained at 20°C. Strains used for live imaging were JJ2330 {ddIs6[pie-1:GFP:TBG-1]; itIs37[pie-1:his-24:mCherry]; stIs10116[his-72:his-24:mCherry]; ltIs44[pie-1:mCherry:PH(PLC1δ1)]} and JJ2418 {ddIs6[pie-1:GFP:TBG-1]; zuIs278[pie-1:mCherry:tba-1]} (Feldman and Priess, 2012). The *C. elegans* strain CB1489 *him-8(e1489)* and the *Rhabditella axei* strain (DF5006) were obtained from the *Caenorhabditis* Genetics Center. *Rhabditis* sp. SB347 and *Rhabditis* sp. JU1783 were kind gifts from Marie-Anne Félix (Institut de Biologie de l'Ecole Normale Supérieure, Paris, France). *Rhabditis* sp. SB372 was from Karin Kiontke (Department of Biology, New York University, USA). SB347 was isolated from a deer tick used as a bait for nematodes (Félix, 2004). SB372 was isolated from a horse dung pile in Freiburg in Germany in August 2003. JU1783 was sampled in La Réunion, in a star fruit, in Melissa domain, Saint-Benoît, in September 2009.

Immunohistochemistry and microscopy

Isolation and antibody labeling of dissected gonads followed established protocols (Shakes et al., 2009). Unless otherwise noted, representative images for the figures were selected from the analysis of spermatocytes from 20-150 male gonads. Primary antibodies included: FITC-conjugated anti-α-tubulin (mouse monoclonal DM1A, Sigma, 1:80), anti-MSP from David Greenstein (Department of Genetics, Cell Biology and Development, University of Minnesota, Minneapolis, USA) (4D5 mouse monoclonal, 1:300; G3197 rabbit polyclonal, 1:15,000), undiluted anti-cyp33-E1 mouse monoclonal (Developmental Studies Hybridoma Bank at the University of Iowa) developed by Hadwiger et al. (2010), anti-GIP-1 [rabbit polyclonal, 1:1000, provided by Anthony Hyman (Hannak et al., 2002)], and anti-IFA [mouse monoclonal, 1:100 (Pruss et al., 1981)]. Affinity-purified secondary antibodies (Jackson ImmunoResearch Laboratories) (1:100) included goat anti-rabbit TRITC-labeled IgG, DyLight 488-labeled goat anti-mouse IgG and Alexa Fluor 488 anti-goat IgM. Actin microfilaments were labeled with rhodamine phalloidin (Molecular Probes). Final slides were mounted with DAPI containing Fluoro Gel II mounting medium (Electron Microscopy Sciences). Images were acquired using an Olympus BX60 microscope using a QImaging EXi Aqua CCD camera. Photos were taken, merged, and exported for analysis using the program iVision. In some cases, the levels adjust function in Adobe Photoshop was used to spread the data containing regions of the image across the full range of tonalities.

Live imaging was performed on a Nikon Ti-E inverted microscope (Nikon Instruments) using a 60× Plan Apochromat objective (NA=1.4) and controlled by NIS Elements software (Nikon). Images were acquired with an Andor Ixon Ultra back thinned EM-CCD camera using 491 nm or 561 nm lasers and a Yokogawa X1 confocal spinning disk head equipped with a 1.5× magnifying lens. Images were taken at a *z*-sampling rate of 0.5 µm and processed in NIS Elements, ImageJ or Adobe Photoshop.

Enhancing the numbers of *R.* sp. SB347 males

Twelve to fifteen dauer larvae, which inevitably develop into hermaphrodites (Chaudhuri et al., 2011), were picked to 60 mm worm plates and allowed to produce a male-enriched early brood (first 12-24 h of egg laying) before removing the adults. Alternatively, dauers were isolated from densely populated but unsynchronized cultures by washing the worms off the plates with ddH_2O, centrifuging the worms, and then treating the worm pellet with 1% w/v SDS in ddH_2O for 30 min at room temperature to kill all worms except the resistant dauer stages. After two washes with ddH_2O, the surviving dauers were transferred to a fresh plate and then removed after they had produced an early brood.

High-pressure freezing, electron microscopy and quantitative image analysis

Three to five males were placed in 1 µl of 20% (w/v) bovine serum albumin in M9 buffer in a hexadecene (Merck)-coated aluminum carrier (cavity 0.1 µm, Art. 241 & 242, Wohlwend, Sennwald, Switzerland). Animals were ultra-

Development (2017) 144, 3253-3263 doi:10.1242/dev.153841

rapidly frozen under high pressure using a Wohlwend HPF Compact 01 (Wohlwend). Freeze-substitution was performed over a period of 3 days at −90°C in anhydrous acetone containing 1% (w/v) OsO_4 and 0.1% (w/v) uranyl acetate using an automated freeze substitution machine (EM AFS, Leica Microsystems). Epon/Araldite-infiltrated worms were flat-embedded in a thin layer of resin, polymerized for 3 days at 60°C and mounted on dummy blocks (Müller-Reichert et al., 2007). Serial thin (70 nm) and semi-thick (300 nm) sections were cut using a Reichert Ultracut S microtome (Leica Microsystems), subsequently collected on Formvar-coated copper slot grids and post-stained with 2% (w/v) uranyl acetate in 70% ethanol followed by 0.4% (w/v) lead citrate. Both sides of grids with semi-thick sections were then covered with 15 nm colloidal gold. The meiotic region within the male worms was located and individual meiotic cells within thin sections were recorded with a TEM (Morgagni 286, FEI) operated at 80 kV. Next, serial semi-thick sections were recorded at a magnification of 2156× with a TEM (EM 906, Zeiss) operated at 80 kV. Consecutive images were registered and stacked with Fiji software (Schindelin et al., 2012). Individual cells were cropped out and analyzed section by section with Fiji. For that, the coordinates of each centrosome was exported, as well as the center of each X chromosome. Then, distances between the two centrosomes and between the X chromosome and the future X-bearing pole were calculated. For quantifying organelles, mitochondria and FB-MOs were counted and assigned either to the non-X (zone Z_1) pole, the X-pole (Z_3), or the region between the poles (zone Z_2).

For electron tomography, dual tilt series of serial semi-thick sections were acquired from −65° to 65° with a 1° increment at a magnification of 4700× with a TEM (Tecnai F30, FEI) operated at 300 kV. The tilt series were reconstructed using the IMOD software package (Kremer et al., 1996). Structures of interest were modeled within the reconstructed volumes using the ZIBAmira software package (Stalling et al., 2005). Microtubules were automatically detected in each section (Weber et al., 2012; Redemann et al., 2014). Next, single microtubule models were combined to represent the whole microtubule network within a cell (Weber et al., 2014). Chromosomes, FB-MOs, mitochondria, Golgi and centrioles were manually segmented.

Acknowledgements

We thank David Greenstein for the anti-MSP antibodies. Some strains were provided by the Caenorhabditis Genetics Center (CGC), which is funded by NIH Office of Research Infrastructure Programs (P40 OD010440). The authors are grateful to Dr Michael Laue (RKI Berlin) for access to the high-pressure freezer.

Competing interests

The authors declare no competing or financial interests.

Author contributions

Conceptualization: E.S.W., G.F., J.L.F., T.M.-R., D.C.S.; Methodology: E.S.W., A.S., G.F., J.L.F., A.P.S., P.L.S., D.C.S.; Formal analysis: E.S.W., A.S., G.F., J.L.F., P.L.S., D.C.S.; Investigation: E.S.W., A.S., G.F., J.L.F., P.L.S., D.C.S.; Resources: D.C.S.; Writing - original draft: D.C.S.; Writing - review & editing: A.S., G.F., J.L.F., A.P.S., T.M.-R., P.L.S., D.C.S.; Supervision: T.M.-R., D.C.S.; Project administration: T.M.-R., D.C.S.; Funding acquisition: J.L.F., A.P.S., T.M.-R., D.C.S.

Funding

This work was supported by grants from the National Institutes of Health (1R155GM096309-0 and DP2GM119136-01 to D.S. and J.F., respectively), from the National Science Foundation (IOS 1122101 to D.C.S. and A.P.S.), from the Biotechnology and Biological Sciences Research Council (BB/L019884/1) to A.P.S., and from the Deutsche Forschungsgemeinschaft (MU 1423/3-2 and MU 1423/10-1 to T.M.-R.). E.S.W. received additional support from the James Monroe Scholars Program, the Mary E. Ferguson Memorial Grant, and a Howard Hughes Medical Institute Undergraduate Science Education Grant to the College of William and Mary. Deposited in PMC for release after 6 months.

Supplementary information

Supplementary information available online at
http://dev.biologists.org/lookup/doi/10.1242/dev.153841.supplemental

References

Albertson, D. G. and Thomson, J. N. (1993). Segregation of holocentric chromosomes at meiosis in the nematode, *Caenorhabditis elegans*. *Chromosome Res.* **1**, 15-26.

Baldi, C., Viviano, J. and Ellis, R. E. (2011). A bias caused by ectopic development produces sexually dimorphic sperm in nematodes. *Curr. Biol.* **21**, 1416-1420.

Bartolini, F. and Gundersen, G. G. (2006). Generation of noncentrosomal microtubule arrays. *J. Cell Sci.* **119**, 4155-4163.

Brenner, S. (1974). The genetics of *Caenorhabditis elegans*. *Genetics* **77**, 71-94.

Campanale, J. P., Sun, T. Y. and Montell, D. J. (2017). Development and dynamics of cell polarity at a glance. *J. Cell Sci.* **130**, 1201-1207.

Chaudhuri, J., Kache, V. and Pires-daSilva, A. (2011). Regulation of sexual plasticity in a nematode that produces males, females, and hermaphrodites. *Curr. Biol.* **21**, 1548-1551.

Chu, D. S. and Shakes, D. C. (2013). Spermatogenesis. *Adv. Exp. Med. Biol.* **757**, 171-203.

Church, D. L., Guan, K. L. and Lambie, E. J. (1995). Three genes of the MAP kinase cascade, *mek-2, mpk-1/sur-1 and let-60 ras*, are required for meiotic cell cycle progression in *Caenorhabditis elegans*. *Development* **121**, 2525-2535.

Clermont, Y. (1972). Kinetics of spermatogenesis in mammals: seminiferous epithelium cycle and spermatogonial renewal. *Physiol. Rev.* **51**, 198-236.

Conduit, P. T., Brunk, K., Dobbelaere, J., Dix, C. I., Lucas, E. P. and Raff, J. W. (2010). Centrioles regulate centrosome size by controlling the rate of Cnn incorporation into the PCM. *Curr. Biol.* **20**, 2178-2186.

Connell, M., Cabernard, C., Ricketson, D., Doe, C. Q. and Prehoda, K. E. (2011). Asymmetric cortical extension shifts cleavage furrow position in Drosophila neuroblasts. *Mol. Biol. Cell* **22**, 4220-4226.

Delaunay, D., Cortay, V., Patti, D., Knoblauch, K. and Dehay, C. (2014). Mitotic spindle asymmetry: a Wnt/PCP-regulated mechanism generating asymmetrical division in cortical precursors. *Cell Rep.* **6**, 400-414.

Fabian, L. and Brill, J. A. (2012). Drosophila spermiogenesis: Big things come from little packages. *Spermatogenesis* **2**, 197-212.

Fabrizio, J. J., Hime, G., Lemmon, S. K. and Bazinet, C. (1998). Genetic dissection of sperm individualization in *Drosophila melanogaster*. *Development* **125**, 1833-1843.

Feldman, J. L. and Priess, J. R. (2012). A role for the centrosome and PAR-3 in the hand-off of MTOC function during epithelial polarization. *Curr. Biol.* **22**, 575-582.

Félix, M. A. (2004). Alternative morphs and plasticity of vulval development in a rhabditid nematode species. *Dev. Genes Evol.* **214**, 55-63.

Hadwiger, G., Dour, S., Arur, S., Fox, P. and Nonet, M. L. (2010). A monoclonal antibody toolkit for *C. elegans*. *PLoS ONE* **5**, e10161.

Halaoui, R. and McCaffrey, L. (2015). Rewiring cell polarity signaling in cancer. *Oncogene* **34**, 939-950.

Hannak, E., Oegema, K., Kirkham, M., Gönczy, P., Habermann, B. and Hyman, A. A. (2002). The kinetically dominant assembly pathway for centrosomal asters in *Caenorhabditis elegans* is gamma-tubulin dependent. *J. Cell Biol.* **157**, 591-602.

Honda, H. (1921). Spermatogenesis of aphids; the fate of the smaller secondary spermatocyte. *Biol. Bull.* **40**, 349-[368]-1.

Januschke, J., Llamazares, S., Reina, J. and Gonzalez, C. (2011). Drosophila neuroblasts retain the daughter centrosome. *Nat. Commun.* **2**, 243.

Justine, J. L. (2002). Male and female gametes and fertilization. In *The Biology of Nematodes* (ed. D. L. Lee), pp. 61-72., Florida: CRC Press.

Kanzaki, N., Kiontke, K., Tanaka, R., Hiooka, Y., Schwarz, A., Müller-Reichert, T., Chaudhura, J. and Pires-daSilva, A. (2017). Description of two three-gendered nematode species in the new genus *Auanema* (Rhabditina) that are models for reproductive mode evolution. *Sci. Rep.* **7**, doi:10.1038/s41598-017-09871-1.

Kelleher, J. F., Mandell, M. A., Moulder, G., Hill, K. L., L'Hernault, S. W., Barstead, R. and Titus, M. A. (2000). Myosin VI is required for asymmetric segregation of cellular components during C. elegans spermatogenesis. *Curr. Biol.* **10**, 1489-1496.

Kiontke, K. and Fitch, D. H. (2005). The phylogenetic relationships of *Caenorhabditis* and other rhabditids. In *WormBook* (ed. The *C. elegans* Research Community), http://www.wormbook.org.

Knoblich, J. A. (2010). Asymmetric cell division: recent developments and their implications for tumour biology. *Nat. Rev. Mol. Cell Biol.* **11**, 849-860.

Kremer, J. R., Mastronarde, J. N. and McIntosh, J. R. (1996). Computer visualization of three-dimensional image data Using IMOD. *J. Struct. Biol.* **116**, 71-76.

Kunda, P., Rodrigues, N. T., Moeendarbary, E., Liu, T., Ivetic, A., Charras, G. and Baum, B. (2012). PP1-mediated moesin dephosphorylation couples polar relaxation to mitotic exit. *Curr. Biol.* **22**, 231-236.

LaMunyon, C. W. and Ward, S. (1999). Evolution of sperm size in nematodes: sperm competition favours larger sperm. *Proc. Biol. Sci.* **266**, 263-267.

Matthews, H. K., Delabre, U., Rohn, J. L., Guck, J., Kunda, P. and Baum, B. (2012). Changes in Ect2 localization couple actomyosin-dependent cell shape changes to mitotic progression. *Dev. Cell* **23**, 371-383.

Müller-Reichert, T., Srayko, M., Hyman, A., O'Toole, E. and McDonald, K. (2007). Correlative light and electron microscopy of early *Caenorhabditis elegans* embryos in mitosis. *Methods Cell Biol.* **79**, 101-119.

Murray, R. L., Kozlowska, J. L. and Cutter, A. D. (2011). Heritable determinants of male fertilization success in the nematode *Caenorhabditis elegans*. *BMC Evol. Biol.* **11**, 99.

Nance, J. and Zallen, J. A. (2011). Elaborating polarity: PAR proteins and the cytoskeleton. *Development* **138**, 799-809.
Nelson, G. A., Roberts, T. M. and Ward, S. (1982). *Caenorhabditis elegans* spermatozoan locomotion: amoeboid movement with almost no actin. *J. Cell Biol.* **92**, 121-131.
Noguchi, T., Lenartowska, M. and Miller, K. G. (2006). Myosin VI stabilizes an actin network during Drosophila spermatid individualization. *Mol. Biol. Cell* **17**, 2559-2571.
O'Donnell, L., Nicholls, P. K., O'Bryan, M. K., McLachlan, R. I. and Stanton, P. G. (2011). Spermiation: the process of sperm release. *Spermatogenesis* **1**, 14-35.
Ou, G., Stuurman, N., D'Ambrosio, M. and Vale, R. D. (2010). Polarized myosin produces unequal-size daughters during asymmetric cell division. *Science* **330**, 677-680.
Pereira, G. and Schiebel, E. (2001). The role of the yeast spindle pole body and the mammalian centrosome in regulating late mitotic events. *Curr. Opin. Cell Biol.* **13**, 762-769.
Peters, N., Perez, D. E., Song, M. H., Liu, Y., Müller-Reichert, T., Caron, C., Kemphues, K. J. and O'Connell, K. F. (2010). Control of mitotic and meiotic centriole duplication by the Plk4-related kinase ZYG-1. *J. Cell Sci.* **123**, 795-805.
Pruss, R. M., Mirsky, R., Raff, M. C., Thorpe, R., Dowding, A. J. and Anderton, B. H. (1981). All classes of intermediate filaments share a common antigenic determinant defined by a monoclonal antibody. *Cell* **27**, 419-428.
Redemann, S., Weber, B., Möller, M., Verbavatz, J. M., Hyman, A. A., Baum, D., Prohaska, S. and Müller-Reichert, T. (2014). The segmentation of microtubules in electron tomograms using Amira. *Methods Mol. Biol.* **1136**, 261-278.
Rodrigues, N. T., Lekomtsev, S., Jananji, S., Kriston-Vizi, J., Hickson, G. R. and Baum, B. (2015). Kinetochore-localized PP1-Sds22 couples chromosome segregation to polar relaxation. *Nature* **524**, 489-492.
Roubinet, C., Decelle, B., Chicanne, G., Dorn, J. F., Payrastre, B., Payre, F. and Carreno, S. (2011). Molecular networks linked by Moesin drive remodeling of the cell cortex during mitosis. *J. Cell Biol.* **195**, 99-112.
Sallee, M. D. and Feldman, J. L. (2015). Flipping the switch: regulating MTOC location. *Cell Cycle* **14**,3519-3520.
Sanchez, A. D. and Feldman, J. L. (2017). Microtubule-organizing centers: from the centrosome to non-centrosomal sites. *Curr. Opin. Cell Biol.* **44**, 93-101.
Schindelin, J., Arganda-Carreras, I., Frise, E., Kaynig, V., Longair, M., Pietzsch, T., Preibisch, S., Rueden, C., Saalfeld, S., Schmid, B. et al. (2012). Fiji: an open-source platform for biological-image analysis. *Nat. Methods* **9**, 676-682.
Shakes, D. C., Wu, J.-c., Sadler, P. L., Laprade, K., Moore, L. L., Noritake, A. and Chu, D. S. (2009). Spermatogenesis-specific features of the meiotic program in *Caenorhabditis elegans*. *PLoS Genet.* **5**, e1000611.
Shakes, D. C., Neva, B. J., Huynh, H., Chaudhuri, J. and Pires-daSilva, A. (2011). Asymmetric spermatocyte division as a mechanism for controlling sex ratios. *Nat. Commun.* **2**, 157.
Sharma, G. P., Gupta, B. L. and Kumbkarni, C. G. (1961). Cytology of spermatogenesis in the honey-bee, *Apis indica* (F.). *J. Microscopy* **79**, 337-351.
Smith, H. (2006). Sperm motility and MSP. In *WormBook* (ed. The *C. elegans* Research Community), http://www.wormbook.org.
Stalling, D., Westerhoff, M. and Hege, H. C. (2005). Amira: a highly interactive system for visual data analysis. In *The Visualization Handbook* (ed. C. D. Hansen and C. R. Johnson), pp. 749-767. Burlington, MA: Elsevier.
Steinhauer, J. (2015). Separating from the pack: molecular mechanisms of Drosophila spermatid individualization. *Spermatogenesis* **5**, e1041345.
Varkey, J. P., Muhlrad, P. J., Minniti, A. N., Do, B. and Ward, S. (1995). The *Caenorhabditis elegans spe-26* gene is necessary to form spermatids and encodes a protein similar to the actin-associated proteins kelch and scruin. *Genes Dev.* **9**, 1074-1086.
Vielle, A., Callemeyn-Torre, N., Gimond, C., Poullet, N., Gray, J. C., Cutter, A. D. and Braendle, C. (2016). Convergent evolution of sperm gigantism and the developmental origins of sperm size variability in *Caenorhabditis* nematodes. *Evolution* **70**, 2485-2503.
Wang, X., Tsai, J. W., Imai, J. H., Lian, W. N., Vallee, R. B. and Shi, S. H. (2009). Asymmetric centrosome inheritance maintains neural progenitors in the neocortex. *Nature* **461**, 947-955.
Ward, S. (1986). Asymmetric localization of gene products during the development of *Caenorhabditis elegans* spermatozoa. In *Gametogenesis and the Early Embryo* (ed. J. G. Gall), pp. 55-75. New York: Alan R. Liss.
Ward, S., Argon, Y. and Nelson, G. A. (1981). Sperm morphogenesis in wild-type and fertilization-defective mutants of *Caenorhabditis elegans*. *J. Cell Biol.* **91**, 26-44.
Weber, B., Greenan, G., Prohaska, S., Baum, D., Hege, H.-C., Müller-Reichert, T., Hyman, A. A. and Verbavatz, J.-M. (2012). Automated tracing of microtubules in electron tomograms of plastic embedded samples of *C. elegans* embryos. *J. Struct. Biol.* **178**, 129-138.
Weber, B., Tranfield, E. M., Höög, J. L., Baum, D., Antony, C., Hyman, T., Verbavatz, J. M. and Prohaska, S. (2014). Automated stitching of microtubule centerlines across serial electron tomograms. *PLoS ONE* **9**, e113222.
Whitney, D. D. (1918). Further studies on the production of functional and rudimentary spermatozoa in rotifers. *Biol. Bull.* **35**, 325-334.
Yamashita, Y. M., Mahowald, A. P., Perlin, J. R. and Fuller, M. T. (2007). Asymmetric inheritance of mother versus daughter centrosome in stem cell division. *Science* **315**, 518-521.
Yi, K., Wang, X., Emmett, M. R., Marshall, A. G., Stewart, M. and Roberts, T. M. (2009). Dephosphorylation of major sperm protein (MSP) fiber protein 3 by protein phosphatase 2A during cell body retraction in the MSP-based amoeboid motility of *Ascaris* sperm. *Mol. Biol. Cell* **20**, 3200-3208.
Yushin, V. V. and Malakhov, V. V. (2014). The origin of nematode sperm: Progenesis at the cellular level. *Russian J. Marine Bio.* **40**, 71-81.
Zhou, K., Rolls, M. M., Hall, D. H., Malone, C. J. and Hanna-Rose, W. (2009). A ZYG-12-dynein interaction at the nuclear envelope defines cytoskeletal architecture in the *C. elegans* gonad. *J. Cell Biol.* **186**, 229-241.